Evidence for Pleistocene gene flow through the ice-free corridor from extinct horses and camels from Natural Trap Cave, Wyoming

Kieren J. Mitchell[a,b,*], Pere Bover[c], Alexander T. Salis[a,d], Caitlin Mudge[a], Holly Heiniger[a], Mary Thompson[e], Bryan Hockett[f], Laura S. Weyrich[a,g,h], Alan Cooper[i,j], Julie A. Meachen[k]

[a] Australian Centre for Ancient DNA, School of Biological Sciences, University of Adelaide, Adelaide, South Australia, Australia

[b] Otago Palaeogenetics Laboratory, Department of Zoology, University of Otago, Dunedin, New Zealand

[c] ARAID Foundation, Instituto Universitario de Investigación en Ciencias Ambientales (IUCA) - Aragosaurus Group, Universidad de Zaragoza, Zaragoza, Spain

[d] Division of Vertebrate Zoology, American Museum of Natural History, New York, New York, USA

[e] Idaho Museum of Natural History, Idaho State University, Idaho, USA

[f] US Department of Interior, Bureau of Land Management, Nevada State Office, Reno, Nevada, USA

[g] Department of Anthropology, Pennsylvania State University, Pennsylvania, USA

[h] Huck Institutes of the Life Sciences, Pennsylvania State University, Pennsylvania, USA

[i] South Australian Museum, Adelaide, South Australia, Australia

[j] BlueSky Genetics, Ashton, South Australia, Australia

[k] Des Moines University, Department of Anatomy, Des Moines, Iowa, USA

* Corresponding author.

E-mail address: kieren.j.mitchell@gmail.com (K.J. Mitchell).

Abstract

Natural Trap Cave (Bighorn Mountains, Wyoming) preserves an abundance of fossil remains from extinct Late Pleistocene fauna and is situated near a past migration route that likely connected populations in Eastern Beringia and the contiguous US—the ice-free corridor between the Cordilleran and Laurentide icesheets. Some palaeontological evidence supports a correspondingly high affinity between fauna recorded in Natural Trap Cave and Eastern Beringia versus elsewhere in the contiguous US, but this hypothesis has not yet been extensively tested using genetic data. In the present study, we analysed 16 horse specimens and one camel specimen from Natural Trap Cave. Of the horse specimens we analysed, we obtained 10 unique and previously unreported mitochondrial haplotypes belonging to two distinct (extinct) genetic clades—two haplotypes corresponded to a caballine horse (*Equus* sp.) and eight corresponded to the stilt-legged horse (*Haringtonhippus francisci*). With only one exception, it appears these newly sequenced individuals all shared a common ancestor more recently with Eastern Beringian individuals than with others from the contiguous US. In addition, mitochondrial data from a specimen assigned to *Camelops* sp. revealed that it shares a closer affinity with specimens from the Yukon Territory than those from Idaho or Nevada, though all appear to belong to a single species (the western camel; *Camelops* cf. *hesternus*). Together, these results are consistent with a high level of genetic connectivity between horse and camel populations in the Bighorn Mountains and Eastern Beringia during the Pleistocene.

Keywords

Phylogenetics; Quaternary; Ancient DNA; Mitogenome; North America; Megafauna

1. Introduction

Throughout the Pleistocene, glacial cycles caused the periodic expansion and contraction of the Cordilleran and Laurentide continental icesheets in the east and west, respectively, of northern North America. During glacial maxima, these two icesheets expanded to the point that they coalesced, likely limiting the dispersal of terrestrial mammals between ice-free areas in Eastern Beringia (Alaska and north-east Canada) and the southern interior of North America (including the modern day contiguous USA). Outside of glacial maxima, an ice-free corridor of varying extent connected these areas and would presumably have permitted faunal dispersal and gene flow. Indeed, fossil data suggest this was the case; for example, morphologically distinct Beringian wolves may have migrated southwards through the ice-free corridor during the Pleistocene prior to the Last Glacial Maximum (Meachen et al., 2016). However, the extent to which the periodic opening and closing of the ice-free corridor influenced the distribution and population structure of

Pleistocene fauna, particularly extinct megafauna, has not been extensively tested using genetic data. Ancient DNA is particularly advantageous for studying this phenomenon, because the ancestry and affinities of ancient individuals—including those from extinct species—can be observed directly rather than inferred. However, application of this approach has been limited by relatively poor DNA preservation in ancient specimens from temperate localities in the contiguous US.

Pleistocene fossils excavated from Natural Trap Cave provide an excellent opportunity to test for past gene flow between animal populations in Eastern Beringia and the North American southern interior (i.e. the contiguous US). Firstly, Natural Trap Cave is situated in the northern Bighorn Mountains, Wyoming, south of the maximum extent of the Pleistocene ice-sheets and very close to the southern terminus of the ice-free corridor (Figure 1). Secondly, fossil remains belonging to a wide range of animal species have been recovered from three distinct periods of deposition—155 to 132 thousand years ago, 53 to 17 thousand years ago, and 11 thousand years ago to the present (Lovelace et al., This issue)—spanning multiple glacial cycles. Finally, previous studies have indicated that ancient DNA can successfully be obtained from fossil remains excavated from Natural Trap Cave (e.g. Barnett et al., 2005; Bover et al., 2018; Heintzman et al., 2016; Heintzman et al., 2017; Orlando et al., 2008; Perri et al., 2021; Salis et al., 2020; Salis et al., 2021; Vershinina et al., 2021). Consequently, if dispersal occurred through the ice-free corridor and resulted in gene flow between populations in Eastern Beringia and the contiguous US, this is likely to be reflected in the ancestry of ancient specimens from Natural Trap Cave. Specifically, we might expect to observe a closer affinity between specimens from Natural Trap Cave and Eastern Beringia, as opposed to those from populations further from the southern terminus of the ice-free corridor. We would also expect shared ancestry between specimens from Natural Trap Cave and Eastern Beringia to date to periods when the ice-free corridor would have been traversable—interglacials (e.g. Marine Isotope Stage 3 [MIS 3]).

Ancient DNA data from North American bison (*Bison* sp.), including specimens from Natural Trap Cave, indicate that bison dispersal through the ice-free corridor likely occurred bi-directionally across multiple glacial cycles (Heintzman et al., 2016). In contrast, the contiguous US appears to have been colonised by brown bears and lions from Eastern Beringia only once, with no evidence for subsequent gene flow (Salis et al., 2020). However, the evidence is less clear-cut either way for other taxa. For example, genetic data have been obtained from the extinct musk-oxen *Bootherium bombifrons*—including specimens from Eastern Beringia, Natural Trap Cave, and as far south as Nebraska—but sampling was too sparse to establish a detailed picture of past dispersal and relatedness through time and space (Bover et al., 2018). Similarly, genetic data from caballine (*Equus*) and stilt-legged (*Haringtonhippus*) horses have been obtained from Natural Trap Cave and other southern localities (Heintzman et al., 2017; Vershinina et al., 2021), but these data are also

relatively sparse and have not specifically been examined in the context of dispersal facilitated by the ice-free corridor.

Both lineages of horse represented at Natural Trap Cave became extinct at the end of the Pleistocene—after the Last Glacial Maximum but prior to the beginning of the Holocene (Heintzman et al., 2017; Lorenzen et al., 2011; Vershinina et al., 2021). As a result, they have no direct modern descendants from which past gene flow can be inferred. Only ancient DNA from temporally and geographically distributed fossil specimens can reveal detailed patterns of population structure and gene flow for these taxa. Similarly, a genus of endemic North American camels (western camels; *Camelops*) became extinct at the end of the Pleistocene (Kooyman et al., 2012; Waters et al., 2015), but it remains unclear exactly how many species this genus comprised (Baskin and Thomas, 2016). Genetic data from three *Camelops* individuals from Eastern Beringia have tentatively been referred to *Camelops hesternus* (Heintzman et al., 2015), but the genetic identity and ancestry of more southern populations currently remains untested. Since all these taxa —*Equus*, *Haringtonhippus*, and *Camelops*—were distributed widely across North American prior to their extinction, including both Eastern Beringia and the contiguous US, they are good models for exploring patterns of past migration through the ice-free corridor.

In this study, we present new mitochondrial genome sequences obtained from 16 horse specimens and one western camel specimen excavated from Late Pleistocene deposits in Natural Trap Cave. Because published genetic data for western camels are otherwise only available from three Eastern Beringian individuals, we also sequenced mitochondrial genomes from two additional specimens for comparison: one from Spider Cave in Idaho and one from Mineral Hill Cave in Nevada. One additional mitochondrial genome was also obtained from a horse specimen from American Falls Reservoir, Idaho. We used these data to better characterise the phylogenetic affinities of horses and camels from Natural Trap Cave with respect to both those from Eastern Beringia and from populations in the contiguous US further from the southern terminus of the ice-free corridor.

2. Material and Methods

2.1 Samples

In this study we analysed DNA from a total of 20 fossil specimens, 17 of which were from Natural Trap Cave. Table S1 lists details for all specimens, including provenance, museum accession numbers, and three newly reported radiocarbon ages. All new and previously published radiocarbon ages were calibrated using OxCal v4.4 (Bronk Ramsey, 2016) based on the IntCal20 calibration curve (Reimer et al., 2020). All pre-PCR genetic research undertaken as part of this

study was conducted in the purpose-built ancient DNA clean-room facilities at the University of Adelaide's Australian Centre for Ancient DNA (ACAD).

2.2 DNA extraction

To reduce contamination, each sample was UV irradiated for 15 min and then the surface layer was abraded using a Dremel tool with a carborundum cutting disc. Each sample was subsequently powdered using a Mikrodismembrator (Sartorius) or fragmented using a BioPulversiser (BioSpec), and 20-200 mg was transferred to a 2 mL screw-cap tube. 1 mL of 0.5 M EDTA was added, and the sample was incubated at room temperature on a rotary mixer for 30-45 min. Samples were then centrifuged, and the EDTA was removed from the screw-cap tube and discarded. An additional 970 μL 0.5 M EDTA and 30 μL 20 mg/mL Proteinase-K were added, and the sample was incubated on a rotary mixer overnight for ~24 hr at 55 ˚C. The DNA released by these digestion steps was bound and purified using a modified version of a previously published method (Dabney et al., 2013), involving a binding step with a buffer comprising 12.6 mL PB buffer (QIAGEN), 6.5 μL Tween-20, and 390 μL NaOAc 3M with in-solution silicon dioxide, followed by two washes with 80% ethanol. Purified DNA was eluted in 200 μL of TE buffer (10 mM Tris, 1 mM EDTA) with 0.05% Tween-20. Negative (no template) controls were included in each batch of samples to monitor background and cross-contamination.

2.3 Library preparation, enrichment, DNA sequencing

Illumina DNA sequencing libraries were made from our extracted DNA and negative controls following the protocol of Meyer and Kircher (2010), but using Rohland et al.'s (2015) partial uracil-DNA-glycosylase (UDG) treatment during the end-polishing step and unique 7-mer 5' and 3' barcoded adapters during the ligation step (Rohland and Reich, 2012). We then performed a real-time PCR assay to determine how many cycles of PCR were required to optimise library quantity and complexity (Gamba et al., 2016). Duplicate real-time PCR assays were performed for each library in a final volume of 10 μL, each comprising 1 μL of a 1:5 dilution of library, 1 x Platinum Taq DNA Polymerase High Fidelity buffer (ThermoFisher Scientific), 2 mM MgSO4 (ThermoFisher Scientific), 0.25 mM of each dNTP (ThermoFisher Scientific), 0.4 μM of each primer (IS7_short_amp_P5 and IS8_short_amp_P7; Meyer and Kircher, 2010), 0.004 x ROX (Life Tech), 0.2 x SYBR (Life Tech), 0.56 M DMSO (Sigma-Aldrich), and 0.2 U of Platinum Taq DNA Polymerase High Fidelity (ThermoFisher Scientific), in laboratory grade water. Real-time PCRs were performed on a LightCycler 96 (Roche) with the following cycling conditions: 94 °C for 6 min; 40 cycles of 94 °C for 30 s, 60 °C for 30 s, 68 °C for 40 s; followed by a high-resolution melt. Results from our rtPCR suggested substantially fewer cycles were required to amplify libraries created from our samples (11-17 cycles) compared with those made from our negative controls

(21-28 cycles), suggesting low DNA template quantities in our controls and negligible levels of cross-contamination.

The libraries were then amplified using conventional PCR. In order to maintain library complexity and minimise PCR bias, each library was amplified in eight separate 25 µL reactions, each comprising 3 µL of undiluted library, 1 x Platinum Taq DNA Polymerase High Fidelity buffer (ThermoFisher Scientific), 2 mM MgSO4 (ThermoFisher Scientific), 0.25 mM of each dNTP (ThermoFisher Scientific), 0.4 µM of each primer (IS7_short_amp_P5 and IS8_short_amp_P7; Meyer and Kircher, 2010), and 0.2 U of Platinum Taq DNA Polymerase High Fidelity (ThermoFisher Scientific), in laboratory grade water. Cycling conditions for the PCR were as follows: 94 °C for 6 min; between 11 and 17 cycles (as determined above using rtPCR) of 94 °C for 30 s, 60 °C for 30 s, 68 °C for 40 s; and 68 °C for 10 min. The exception was the library made for UW51516, which was subjected to Recombinase Polymerase Amplification (RPA) for 40 min using a TwistAmp Basic kit (TwistDx Inc.) and following the manufacturer's protocol. Amplified libraries were pooled and purified using 1.8 x volume AxyPrep (Axygen), washed twice with 80% ethanol, and then resuspended in 30 µL of buffer comprising 10 mM Tris, 0.1 mM EDTA, and 0.05% Tween-20.

All libraries were enriched for placental mammal mitochondrial DNA using hybridisation enrichment with the commercially synthesised RNA probes described by Mitchell et al. (2016). Hybridisation enrichment was performed according to the manufacturer's protocol (Arbor Biosciences: myBaits v3 chemistry) with several modifications: (1) we extended the incubation step to 44 hr (15 hr at 55 °C, 16 hr at 50 °C, 17 hr at 55 °C); (2) we used RNA blockers complementary to our truncated library adapters instead of the Blocker #3 provided by the manufacturer; (3) prior to immobilising the RNA baits, we incubated the Dynabeads MyOne Streptavidin C1 (ThermoFisher Scientific) with 100 µg of yeast tRNA to saturate bead sites that bind nucleic acids in a non-specific manner (Llamas et al., 2016); and (4) we washed the RNA baits—once bound to the streptavidin beads—three times by incubating for 5 min at 55 °C with 0.1 SSC and 0.1% SDS (discarding the supernatant after each wash).

Following, post-enrichment purification, all libraries were eluted in 125uL of PCR master mix (1 × PCR buffer, 2.5 mM MgCl2, 1 mM dNTPs, 0.5 mM primer, 6.25 U AmpliTaq Gold). The master mix from each library was then split into five reactions and subjected to the following thermocycling regime: 94 °C 6 min; 15 cycles of 94 °C for 30 s, 60 °C for 30 s, 72 °C for 45 s; and a final extension of 72 °C for 10 min. Forward and reverse primers included full-length indexed Illumina sequencing adapters (see Meyer and Kircher, 2010). PCR products from each library were pooled and purified using 1.1 x volume AxyPrep (Axygen), washed twice with 80% ethanol, and then resuspended in 30 µL of water.

2.4 High-throughput sequencing and data processing

All libraries were pooled and sequenced together on either an Illumina NextSeq or HiSeq in paired-end sequencing mode. Raw sequencing reads were demultiplexed using "sabre" (http://github.com/najoshi/sabre) according to their unique 7-mer barcode combinations. Using AdapterRemoval v2.1.2 (Schubert et al., 2016) we trimmed residual adapters and low-quality bases (<Phred20 –minquality 4); merged overlapping paired-end reads (minimum overlap = 11 nt); and discarded merged reads <30 bp (–minlength 30). Read quality was visualised using fastQC v0.10.1 (https://www.bioinformatics.babraham.ac.uk/projects/fastqc/) before and after trimming to make sure the trimming was efficient.

Mitochondrial consensus sequences were obtained by mapping all merged reads for each library against a previously published reference sequence for their respective species—KT168321 for stilt-legged horses, KT168318 for caballine horses, and KR822421 for western camels—using BWA v0.7.8 (Li and Durbin, 2009; aln -t 8 -l 1024 -n 0.04 -o 2). Reads with a mapping quality Phred score >30 were selected and retained using the SAMtools v1.4 (Li et al., 2009) view command (-q 30), and duplicate reads were discarded using 'FilterUniqueSAMCons.py' (Kircher, 2012). A final 75% majority consensus sequence was then generated for each library and checked by eye in Geneious v9.1.6 (https://www.geneious.com), calling nucleotides for sites with a minimum depth-of-coverage of 3x. Summary statistics for each consensus sequences are provided in Table S1.

2.5 Phylogenetic analyses

We aligned our new mitochondrial genome sequences with previously published data (Table S1) using the MUSCLE v3.8.425 (Edgar, 2004) algorithm as implemented in Geneious. Three separate alignments were created: one for stilt-legged horses (n=39; 16,655 bp), one for caballine horses (n=34; 16,662 bp), and one for western camels (n=6; 16,681 bp). Ambiguously aligned columns were removed using Gblocks v0.91b (Castresana, 2000) with default settings, which reduced the length of our caballine horse alignment to 16,317 bp. We inferred maximum likelihood phylogenies based on our stilt-legged and caballine horse alignments using IQ-TREE v1.6.11 (Nguyen et al., 2015), with the best-fitting substitution model (HKY+I) selected using ModelFinder (according to the Bayesian Information Criterion) as implemented in IQ-TREE (Kalyaanamoorthy et al., 2017) and 1000 ultrafast bootstrap replicates to assess topological support (Hoang et al., 2017). We created a median-joining haplotype network (Bandelt et al., 1999) from our western camel alignment using PopART v1.7 (Leigh and Bryant, 2015).

We used BEAST v1.8.4 (Drummond and Rambaut, 2007) to co-estimate phylogenies, node ages, and tip ages (for specimens without ages measured using radiocarbon dating) using our stilt-legged and caballine horse alignments. We first evaluated the temporal signal in these two alignments using leave-one-out cross-validation (see Stiller et al., 2014) after pruning our alignment to only the sequences from specimens with finite radiocarbon ages (18 stilt-legged horses and 23 caballine horses; see Table S1). Cross validation involved a series of analyses wherein the age of each sample was sequentially omitted and estimated (applying a uniform prior of 0-150 ka—reflecting a range of plausible deposition ages—instead of specifying the radiocarbon age of the specimen). In each case, we applied the best fitting model estimated previously using IQ-TREE (HKY+I), used a strict molecular clock model, and applied a constant population size coalescent tree prior. A uniform prior of 10^{-11} to 10^{-5} substitutions per site per year was placed on the clock rate. The Markov chain Monte Carlo (MCMC) was run for 2×10^6 generations sampling trees and parameter values every 2000 generations. Convergence of parameter values and ESSs > 200 were monitored using Tracer v1.7.1 (Rambaut et al., 2018). For all except one caballine horse, the calibrated radiocarbon age fell within the 95% Highest Posterior Density (95% HPD) of the Bayesian estimate (Table S1), suggesting that our data collectively included sufficient temporal information to estimate the age of undated samples. For the one caballine horse sample that failed cross-validation (IMNH 1136/11898), the estimated age (median = 52.5 ka; 95% HPD = 33.3ka – 74.7 ka) was substantially older than the calibrated radiocarbon age (median = 17275 cal BP; CAMS_LLNL-175552), possibly due to contamination of the sample with relatively young carbon (e.g. from adhesives or consolidants; Crann and Grant, 2019) that was not removed prior to radiocarbon dating; as a result, we used the median estimated age from BEAST for this one specimen in all downstream analyses.

We subsequently performed another series of BEAST analyses wherein those sequences from horse specimens without radiocarbon ages or with infinite radiocarbon ages were sequentially and individually added into their respective alignments in order to estimate the age of the specimens (applying a uniform prior of 0-150 ka on the unknown age). Otherwise, these runs used the same priors and MCMC settings as for the cross-validation analyses described above. Two stilt-legged horse sequences were excluded at this point because their position in the tree precluded accurate date estimate (they were an outgroup to all directly dated samples; Figure 2A). Once all other samples were assigned an age (either based on radiocarbon dating or Bayesian date estimation), we conducted a date-randomisation test for each alignment (Ramsden et al., 2008; Stiller et al., 2014). The date randomisation tests involved assigning each sample an age from the set of all sample ages (sampling without replacement), which we did by extracting the sample ages from our BEAST XML files, re-ordering them according to a randomly assigned integer, and then re-assigning the re-ordered ages to the samples as they were ordered in the original BEAST XML file. For both alignments the posterior substitution rate estimate of the original data did not overlap the

95% HPDs of the rate estimates from ten such randomised replicates, suggesting that our dataset could be used to reliably estimate evolutionary rate and divergence times (Figure S1). Again, these date randomisation runs used the same priors and MCMC settings as for the cross-validation.

We then ran two final BEAST analyses for our stilt-legged horse and caballine horse alignments. These analyses were run as above, except we used an Extended Bayesian Skyline coalescent tree prior, posterior medians for the age of sequences without finite radiocarbon ages, and three separate MCMCs. After removing the first 10% of values sampled by each MCMC, we combined the remaining samples using LogCombiner v1.8.4 and created a maximum clade credibility tree using TreeAnnotator v1.8.4. Convergence of parameter values between the three chains and combined effective sample sizes > 200 were assessed using Tracer v1.7.1. We observed that the inclusion of several sequences in each alignment with >20% indeterminate nucleotides (i.e. coded as N) were contributing to topological uncertainty—reducing branch support across the tree—so we excluded these from our final BEAST analyses (see Table S1; Figure 2A, 3A). Consequently, our final alignments for stilt-legged and caballine horses comprised 32 sequences each.

In addition to analyses of our horse alignments, we also ran a BEAST analysis for our western camel alignment. However, because that alignment only contained six sequences—including only three specimens with finite radiocarbon ages (Table S1)—we could not perform the cross-validation or date randomisation tests described above for the stilt-legged and caballine horses. Instead, we constrained the age of the three Eastern Beringian camel specimens with infinite radiocarbon ages using uniform distributions from 50 to 150 ka. We also placed a uniform distribution on the substitution rate of 5.0×10^{-9} to 4.0×10^{-8} substitutions per site per year, which spans a range of values typical for large terrestrial mammals, and we used a constant population size coalescent tree prior. Three separate MCMCs were run for 10^6 generations sampling trees and parameter values every 1000 generations. Otherwise, this analysis was performed using the same settings as for our final analyses of the horse alignments and results were summarised in the same way. Importantly, the posterior ages estimated for camels in this study should only be taken as indicative until they are subject to more rigorous analyses with larger sample sizes that allow for internal validation.

3. Results and Discussion

3.1 Stilt-legged horses (Haringtonhippus)

Of the 16 horse specimens from Natural Trap Cave that we analysed, 13 yielded mitochondrial haplotypes that showed a close affinity for published sequences from the stilt-legged horse, *Haringtonhippus francisci* (Figure 2A). Eight of these new haplotypes were unique, with the

remaining five plausibly representing different specimens from the same individual animals. These eight new haplotypes were all distinct from sequences published by Heintzman et al. (2017), which brings the total number of unique *Haringtonhippus* haplotypes—effectively equivalent to the minimum number of individuals—known from Natural Trap Cave to 14.

The results of our phylogenetic analyses revealed that 11 of our 13 new *Haringtonhippus* sequences fall within the mitochondrial diversity described by Heintzman et al. (2017), though sequences from Natural Trap Cave do not form a monophyletic clade to the exclusion of sequences from Eastern Beringia or Nevada (Figure 2A). The remaining two sequences—comprising a single unique haplotype—may represent a sister-lineage to all other sequences (Figure 2A). In our view, the genetic distance between these two outgroup sequences and the remaining sequences is unlikely to be of taxonomic significance, although that hypothesis could be tested more rigorously in the future with additional data. Currently, these outgroup specimens have not been directly radiocarbon dated and are also excluded from the results of our Bayesian analysis because the long branch separating them from the remaining samples caused problems with date estimation and convergence of the MCMC (see Section 2.5; Table S1).

All of the stilt-legged horse sequences from Natural Trap Cave included in our final Bayesian analysis shared a common ancestor more recently with a sequence from Eastern Beringia, and *vice versa*, than with any of the three sequences previously reported from Gypsum Cave in Nevada (Bayesian posterior probability, BPP = 1.0; Figure 2B). This pattern is consistent with ongoing gene flow between Eastern Beringian stilt-legged horse populations and those near to Natural Trap Cave during the Pleistocene, though uncertainty associated with our node age estimates makes the precise timeframe unclear. In addition, high levels of missing data prevented us from confidently determining the affinities of six additional specimens from Natural Trap Cave and one specimen from Mineral Hill Cave, Nevada (see Section 2.5, Figure 2A, Table S1). Consequently, while our results may be suggestive, it is difficult to draw firm conclusions about the connectivity of stilt-legged horse populations in Eastern Beringia and near Natural Trap Cave with those further from the southern terminus of the ice-free corridor (e.g. those in Nevada; Figure 1).

3.2 Caballine horses (Equus)

Three of our horse specimens from Natural Trap cave yielded caballine horse (*Equus*) mitochondrial haplotypes (Figure 3A) – only two of these were unique, suggesting that they may represent only two different individuals. Vershinina et al. (2021) recently reported caballine horse mitochondrial genome sequences from another four specimens from Natural Trap Cave; however, three of their sequences are identical and could plausibly represent multiple specimens from a single individual animal, especially since radiocarbon ages for all three specimens are practically

indistinguishable. Our new data therefore bring the total number of unique caballine horse haplotypes known from Natural Trap Cave to four, which all belong to Vershinina et al.'s (2021) "clade B". Consequently, we only included clade B haplotypes in our downstream analyses. Within North America, clade A haplotypes—specifically A1 and A2 haplotypes—have been reported only from Eastern Beringia and appear to derive from eastward migration across the Bering Land Bridge from Eurasia between 50 and 200 ka (Vershinina et al., 2021).

As with the stilt-legged horses (Section 3.1, Figure 2), we observed no close affinity between caballine horse sequences from Natural Trap Cave and those obtained from specimens elsewhere in the contiguous US (Figure 3)—represented in our analyses by two sequences from Idaho (one of which we sequenced as part of this study). Instead, one of our new Natural Trap Cave sequences formed a clade with one of Vershinina et al.'s (2021) Natural Trap Cave sequences (BPP = 1.0), which in turn shared a more recent common ancestor with a sequence from Eastern Beringia (BPP = 0.94; Figure 3B), while the remaining two of our new Natural Trap Cave sequences were excluded from our final analysis due to high levels of missing data (see Section 2.5, Table S1, Figure 3A). In contrast, Vershinina et al.'s (2021) remaining three sequences from Natural Trap Cave represent a relatively distinct lineage, which last shared a common ancestor with other sequences >100 ka; as for similarly distinct stilt-legged horse lineages from Natural Trap Cave (Section 3.1), this distinct caballine horse lineage may indicate persistent local phylogeographic structure in addition to gene flow with populations in Eastern Beringia.

Unlike the stilt-legged horse samples from Nevada, which were all closely related (Figure 2), the caballine horse sequences from Idaho were the respective sister lineages to two distinct clades otherwise comprising samples from Eastern Beringia and Natural Trap Cave or Alberta (BPP = 0.94 & 1.0, respectively; Figure 3B). The majority of node age estimates within these clades—including the common ancestors of our new Natural Trap Cave sequence and its nearest Eastern Beringian relative—fall within Marine Isotope Stage 3 (MIS 3; 29-57 ka; Figure 3B), when an ice-free corridor was likely present. This is consistent with the occurrence of gene flow between horse populations in Eastern Beringia and those near to Natural Trap Cave via the ice-free corridor prior to coalescence of the ice-sheets during the Last Glacial Maximum. However, age estimates for the common ancestors between these clades and their respective nearest relatives from Idaho (95% HPDs = 65.1-84.9 ka & 50.5-65.9 ka, respectively) substantially overlap with MIS 4 (57-71 ka), when the ice-free corridor may have been inaccessible or less traversable. Together, these observations suggest that populations in the contiguous US, particularly those near to Natural Trap Cave, may have been the source of *Equus* clade B diversity observed in Eastern Beringia during MIS 3, with the majority of gene flow occurring from south to north. This hypothesis is further supported by the apparent absence of *Equus* clade A1 and A2 haplotypes from the contiguous US

—otherwise found only in Eastern Beringia—despite increasing the number of samples that were examined by Vershinina et al. (2021).

3.3 Western camel (Camelops)

Our Bayesian phylogenetic analysis of the western camel (*Camelops* sp.) included sequences from six specimens: three from Eastern Beringia published by Heintzman et al. (2015), one from Natural Trap Cave, one from Spider Cave in Idaho, and one from Mineral Hill Cave in Nevada (Figure 4A). Our results strongly supported reciprocal monophyly of a clade comprising the sequences from Idaho and Nevada (BPP = 1.0) and a clade comprising the Eastern Beringian sequences and the sequence from Natural Trap Cave (BPP = 1.0). The common ancestor of these two clades occurred between 213 and 836 ka (95% HPD; median = 405 ka; Figure 4B), suggesting that they all likely belong to a single species (*Camelops* cf. *hesternus*; Heintzman et al., 2015). However, our node age estimates for *Camelops* are relatively imprecise and should be treated with caution because they were not estimated using as informative or objective priors compared to our analyses of caballine and stilt-legged horses (see Section 2.5).

The camel sample from Natural Trap Cave was most closely related to one of the Eastern Beringian samples—YG 328.23—to the exclusion of the remaining two (Figure 4). Our results suggest that the common ancestor of the Natural Trap Cave specimen and its nearest relative occurred between 65.3 and 195 ka (95% HPD; median = 122 ka; Figure 4B). As for the horses (Sections 3.1 & 3.2), this pattern is consistent with greater population connectivity and gene flow between Eastern Beringian populations and those near to Natural Trap Cave versus populations in the contiguous US further from the southern terminus of the ice-free corridor. However, because our dataset includes very few individuals—as for a previous study the extinct musk-oxen *Bootherium bombifrons* (Bover et al., 2018)—this result may be a sampling artefact and needs to be confirmed in the future with more comprehensive sampling.

3.4 Synthesis

Contrary to previous work that suggested as many as four distinct horse species were represented among the Pleistocene fossils from Natural Trap Cave (e.g. Eisenmann et al., 2008), genetic data to date—including our new sequences—only provide strong evidence for two species: one species of stilt-legged horse (*Haringtonhippus francisci*) and one species of caballine horse (*Equus* sp.). This conclusion remains true even if the wider mitochondrial diversity described by Vershinina et al. (2021) is interpreted as corresponding to several distinct species (e.g. *Equus ferus*, *E. lambei*, *E. scotti*, *E. occidentalis*), because sequences from Natural Trap Cave all belong to a relatively restricted subset of overall caballine horse diversity (“clade B”; Figure 3). Additional sampling may

yet reveal genetic evidence for additional lineages at Natural Trap Cave, but if so they must occur only at very low abundance, having not been detected among the 18 unique horse haplotypes thus far obtained. With respect to abundances, we also note that—assuming horse samples have been randomly chosen for genetic analysis—genetic data are consistent with a roughly three-fold higher abundance of stilt-legged horses versus caballine horses in the Natural Trap Cave assemblage.

Overall, our results from stilt-legged horses, caballine horses, and western camels are all consistent with a higher level of connectivity between populations in Eastern Beringia and those near Natural Trap Cave during the Pleistocene when compared with populations further from the southern terminus of the ice-free corridor (e.g. those in Idaho or Nevada; Figure 1). However, the strength of this conclusion is limited by sparse sampling from localities in the contiguous US other than Natural Trap Cave and the imprecision of our node age estimates, specifically for stilt-legged horses and western camels. Greater sampling intensity in future studies may overcome these limitations. Hall's Cave in Texas, where short fragments of DNA from both *Camelops* and *Haringtonhippus* have been detected in bulk bone samples (Seersholm et al., 2020), may be a promising site for expanding the geographical breadth of datasets for these species. The inclusion of nuclear DNA—if it can reliably be obtained from specimens from the contiguous US—would also help to reveal evidence for finer-scale gene flow that is not captured in the mitochondrial phylogeny of these taxa. Nevertheless, our data reveal intriguing patterns, specifically the lack of strong evidence for southward versus northward dispersal of caballine horses through the ice-free corridor during MIS3. This contrasts with data from bison, brown bears, and lions, which suggest dispersal of these taxa through the ice-free corridor occurred primarily from Eastern Beringia into the contiguous US (Heintzman et al., 2016; Salis et al., 2020), emphasising that patterns of megafaunal dispersal during the Pleistocene are species specific. It may therefore be illuminating to expand sampling of ancient DNA from the contiguous US—including Natural Trap Cave—to include taxa like grey wolves and bighorn sheep, which may also have traversed the ice-free corridor (e.g. Meachen et al., 2016).

Author contributions

Conceptualisation: KJM, AC, JAM; Investigation: KJM, CM, PB, ATS, HH; Formal analysis: KJM; Data Curation: KJM, CM, PB, ATS, HH, JAM, MT, BH; Resources: KJM, AC, LSW, JAM, MT, BH; Visualisation and Writing (Original Draft): KJM; Writing (Review & Editing): all authors; Funding acquisition: AC, JAM.

Data availability

Mitochondrial consensus sequences produced as part of this study are available on GenBank (TBA-TBA). Consensus sequences, demultiplexed sequencing reads, and phylogenetic analysis files—including BEAST XMLs—are available through figshare (DOI: TBA).

Declaration of competing interests

The authors declare that they have no known competing financial interests or personal relationships that could have appeared to influence the work reported in this paper.

Acknowledgements

We thank the following individuals and organisations for providing permission to analyse samples: Idaho Museum of Natural History, Bureau of Land Management (Brent Breithaupt and Gretchen Hurley), University of Kansas Vertebrate Paleontology, and the University of Wyoming. Samples held by the University of Wyoming were collected from Natural Trap Cave under permit PA13-WY-207 awarded to JAM.

Funding

Funding for this research was awarded to JAM and AC by the US National Science Foundation (grant EAR/SGP# 1425059) and to AC by the Australian Research Council (grant FL140100260).

Figure captions

Figure 1 (colour): Map of study areas relative to the location of the Cordilleran and Laurentide ice sheets and the ice-free corridor connecting Eastern Beringia (dark gray) from locations in the contiguous US (adapted from Meachen et al., 2016). Depiction approximates extent during Pleistocene glacial minima; during glacial maxima the ice sheets would likely have coalesced and no ice-free corridor would have been present. Natural Trap Cave (blue circle) in Wyoming (blue) is closer to the southern terminus of the ice-free corridor compared to study sites in Idaho (orange; light and dark orange circles) or Nevada (red; light and dark red circles).

Figure 2 (colour): A) Maximum likelihood phylogeny of stilt-legged horse (*Haringtonhippus francisci*) mitochondrial genome sequences. Ultrafast bootstrap support from IQ-TREE is displayed for nodes with 95% support or higher. Tips are labelled with a shorthand reference number (see Table S1) and specimen ID; new sequences obtained as part of this study are marked with an asterisk. Coloured circles indicate geographical provenance of samples. Branch lengths are proportional to number of substitutions; scale is in number of substitutions per site. Sequences

labelled in grey were excluded from our final Bayesian analysis (see Section 2.5; Table S1). **B)** Time-calibrated Bayesian phylogeny of stilt-legged horse mitochondrial genome sequences. Coloured circles indicate geographical distribution of samples. Samples are labelled with a shorthand reference (see Table S1); new sequences are marked with an asterisk. Shaded vertical bars demarcate Marine Isotope Stages 1 through 7 (even numbered MISs are colder glacials while odd numbered MISs are warmer interglacials). Branch lengths are proportional to time (scaled in thousands of years before present). Tip and node heights are plotted as median values. Horizontal node bars reflect 95% Highest Posterior Densities (95% HPDs). Labels reflect Bayesian posterior probability (only displayed for branches with a value of at least 0.90).

Figure 3 (colour): A) Maximum likelihood phylogeny of caballine horse mitochondrial genome sequences corresponding to Vershinina et al.'s (2021) *Equus* sp. "clade B". Ultrafast bootstrap support from IQ-TREE is displayed for nodes with 95% support or higher. Tips are labelled with a shorthand reference number (see Table S1) and specimen ID; new sequences obtained as part of this study are marked with an asterisk. Coloured circles indicate geographical provenance of samples. Branch lengths are proportional to number of substitutions; scale is in number of substitutions per site. Sequences labelled in grey were excluded from our final Bayesian analysis because they comprised a high number of indeterminate nucleotides (see Section 2.5; Table S1). **B)** Time-calibrated Bayesian phylogeny of caballine horse mitochondrial genome sequences. Coloured circles indicate geographical distribution of samples. New sequences are marked with an asterisk. Shaded bars demarcate Marine Isotope Stages 1 through 6 (even numbered MISs are colder glacials while odd numbered MISs are warmer interglacials). Branch lengths are proportional to time (scaled in thousands of years before present). Tip and node heights are plotted as median values. Node bars reflect 95% Highest Posterior Densities (95% HPDs). Labels reflect Bayesian posterior probability (only displayed for branches with a value of at least 0.90).

Figure 4 (colour): A) Median-joining haplotype network for western camel (*Camelops* sp.) mitochondrial genome sequences from Natural Trap Cave (blue circle), Spider Cave (orange circle), Mineral Hill Cave (red circle), and Eastern Beringia (grey circle). Tips are labelled in with a shorthand reference number (see Table S1) and new sequences are marked with an asterisk. Network edges are labelled with the number of substitutions separating haplotypes. B) Time-calibrated Bayesian phylogeny of western camel mitochondrial genome sequences. Branch lengths are proportional to time (in thousands of years before present); tip and node heights are median values; node bars reflect 95% Highest Posterior Densities (95% HPDs). Labels reflect Bayesian posterior probability.

Supplementary data captions

Table S1: Provenance, age, and genetic metadata for all specimens analysed in this study.

Figure S1: Results of BEAST date randomisation tests for our stilt-legged horse (left) and caballine horse (right) alignments. The first column in each plot is the substitution rate estimated using the "true data" i.e. all samples assigned their correct age. The remaining columns in each plot are the substitution rate estimated using datasets where sample ages are randomly assigned to samples (without replacement). The central line represents the mean value, boxes represent the 95% Highest Posterior Density (95% HPD), and whiskers represent the range. 95% HPDs do not overlap between the true data and the randomised replicates, indicating that each dataset encompasses significant temporal information.

References

Bandelt HJ, Forster P, Röhl A. 1999. Median-joining networks for inferring intraspecific phylogenies. Mol Biol Evol 16(1):37-48.

Barnett R, Barnes I, Phillips MJ, Martin LD, Harington CR, Leonard JA, Cooper A. 2005. Evolution of the extinct sabretooths and the American cheetah-like cat. Curr Biol 15(15):R589-R590.

Baskin J, Thomas R. 2016. A review of Camelops (Mammalia, Artiodactyla, Camelidae), a giant llama from the Middle and Late Pleistocene (Irvingtonian and Rancholabrean) of North America. Hist Biol 28(1-2):120-127.

Bover P, Llamas B, Thomson VA, Pons J, Cooper A, Mitchell KJ. 2018. Molecular resolution to a morphological controversy: The case of North American fossil muskoxen Bootherium and Symbos. Mol Phylogenet Evol 129:70-76.

Bronk Ramsey C. 2016. Bayesian Analysis of Radiocarbon Dates. Radiocarbon 51(1):337-360.

Castresana J. 2000. Selection of Conserved Blocks from Multiple Alignments for Their Use in Phylogenetic Analysis. Mol Biol Evol 17(4):540-552.

Crann CA, Grant T. 2019. Radiocarbon age of consolidants and adhesives used in archaeological conservation. Journal of Archaeological Science: Reports 24:1059-1063.

Dabney J, Knapp M, Glocke I, Gansauge M-T, Weihmann A, Nickel B, Valdiosera C, García N, Pääbo S, Arsuaga J-L, Meyer M. 2013. Complete mitochondrial genome sequence of a Middle Pleistocene cave bear reconstructed from ultrashort DNA fragments. Proceedings of the National Academy of Sciences 110(39):15758-15763.

Drummond AJ, Rambaut A. 2007. BEAST: Bayesian evolutionary analysis by sampling trees. BMC Evol Biol 7(214).

Edgar RC. 2004. MUSCLE: multiple sequence alignment with high accuracy and high throughput. Nucleic Acids Res 32(5):1792-1797.

Eisenmann V, Howe J, Pichardo M. 2008. Old world hemiones and new world slender species (Mammalia, Equidae). Palaeovertebrata 36:159-233.

Gamba C, Hanghøj K, Gaunitz C, Alfarhan AH, Alquraishi SA, Al-Rasheid KAS, Bradley DG, Orlando L. 2016. Comparing the performance of three ancient DNA extraction methods for high-throughput sequencing. Molecular Ecology Resources 16(2):459-469.

Heintzman PD, Froese D, Ives JW, Soares AER, Zazula GD, Letts B, Andrews TD, Driver JC, Hall E, Hare PG, Jass CN, MacKay G, Southon JR, Stiller M, Woywitka R, Suchard MA, Shapiro B. 2016. Bison phylogeography constrains dispersal and viability of the Ice Free Corridor in western Canada. Proc Natl Acad Sci U S A 113(29):8057-8063.

Heintzman PD, Zazula GD, Cahill JA, Reyes AV, MacPhee RDE, Shapiro B. 2015. Genomic Data from Extinct North American Camelops Revise Camel Evolutionary History. Mol Biol Evol 32(9):2433-2440.

Heintzman PD, Zazula GD, MacPhee RDE, Scott E, Cahill JA, McHorse BK, Kapp JD, Stiller M, Wooller MJ, Orlando L, Southon J, Froese DG, Shapiro B. 2017. A new genus of horse from Pleistocene North America. eLife 6:e29944.

Hoang DT, Chernomor O, von Haeseler A, Minh BQ, Vinh LS. 2017. UFBoot2: Improving the Ultrafast Bootstrap Approximation. Mol Biol Evol 35(2):518-522.

Kalyaanamoorthy S, Minh BQ, Wong TKF, von Haeseler A, Jermiin LS. 2017. ModelFinder: fast model selection for accurate phylogenetic estimates. Nature methods 14(6):587-589.

Kircher M. 2012. Analysis of High-Throughput Ancient DNA Sequencing Data. Ancient DNA: Methods and Protocols. p 197-228.

Kooyman B, Hills LV, Tolman S, McNeil P. 2012. LATE PLEISTOCENE WESTERN CAMEL (CAMELOPS HESTERNUS) HUNTING IN SOUTHWESTERN CANADA. Am Antiq 77(1):115-124.

Leigh JW, Bryant D. 2015. popart: full-feature software for haplotype network construction. Methods in Ecology and Evolution 6(9):1110-1116.

Li H, Durbin R. 2009. Fast and accurate short read alignment with Burrows-Wheeler transform. Bioinformatics 25(14):1754-1760.

Li H, Handsaker B, Wysoker A, Fennell T, Ruan J, Homer N, Marth G, Abecasis G, Durbin R, Subgroup GPDP. 2009. The Sequence Alignment/Map (SAM) format and SAMtools. Bioinformatics 25(16):2078-2079.

Llamas B, Fehren-Schmitz L, Valverde G, Soubrier J, Mallick S, Rohland N, Nordenfelt S, Valdiosera C, Richards SM, Rohrlach A, Romero MIB, Espinoza IF, Cagigao ET, Jiménez LW, Makowski K, Reyna ISL, Lory JM, Torrez JAB, Rivera MA, Burger RL, Ceruti MC, Reinhard J, Wells RS, Politis G, Santoro CM, Standen VG, Smith C, Reich D, Ho SYW, Cooper A, Haak W. 2016. Ancient mitochondrial DNA provides high-resolution time scale of the peopling of the Americas. Science Advances 2(4).

Lorenzen ED, Nogues-Bravo D, Orlando L, Weinstock J, Binladen J, Marske KA, Ugan A, Borregaard MK, Gilbert MT, Nielsen R, Ho SY, Goebel T, Graf KE, Byers D, Stenderup JT, Rasmussen M, Campos PF, Leonard JA, Koepfli KP, Froese D, Zazula G, Stafford TW, Jr.,

642 Aaris-Sorensen K, Batra P, Haywood AM, Singarayer JS, Valdes PJ, Boeskorov G, Burns
643 JA, Davydov SP, Haile J, Jenkins DL, Kosintsev P, Kuznetsova T, Lai X, Martin LD,
644 McDonald HG, Mol D, Meldgaard M, Munch K, Stephan E, Sablin M, Sommer RS, Sipko T,
645 Scott E, Suchard MA, Tikhonov A, Willerslev R, Wayne RK, Cooper A, Hofreiter M, Sher A,
646 Shapiro B, Rahbek C, Willerslev E. 2011. Species-specific responses of Late Quaternary
647 megafauna to climate and humans. Nature 479(7373):359-364.
648 Lovelace DM, Redman CM, Minckley TA, Schubert BW, Mahan S, Wood JR, McGuire JL, Laden J,
649 Bitterman K, Heiniger H, Fenderson L, Cooper A, Mitchell KJ, Meachen JA. This issue. An
650 age-depth model and revised stratigraphy of vertebrate-bearing units in Natural Trap Cave,
651 Wyoming. Quat Int.
652 Meachen JA, Brannick AL, Fry TJ. 2016. Extinct Beringian wolf morphotype found in the
653 continental U.S. has implications for wolf migration and evolution. Ecology and Evolution
654 6(10):3430-3438.
655 Meyer M, Kircher M. 2010. Illumina sequencing library preparation for highly multiplexed target
656 capture and sequencing. Cold Spring Harbor Protocols 2010(6):1-10.
657 Mitchell KJ, Bray SC, Bover P, Soibelzon L, Schubert BW, Prevosti F, Prieto A, Martin F, Austin JJ,
658 Cooper A. 2016. Ancient mitochondrial DNA reveals convergent evolution of giant short-
659 faced bears (Tremarctinae) in North and South America. Biol Lett 12(4).
660 Nguyen LT, Schmidt HA, von Haeseler A, Minh BQ. 2015. IQ-TREE: a fast and effective stochastic
661 algorithm for estimating maximum-likelihood phylogenies. Mol Biol Evol 32(1):268-274.
662 Orlando L, Male D, Alberdi MT, Prado JL, Prieto A, Cooper A, Hanni C. 2008. Ancient DNA
663 clarifies the evolutionary history of American late Pleistocene equids. J Mol Evol 66(5):533-
664 538.
665 Perri AR, Mitchell KJ, Mouton A, Álvarez-Carretero S, Hulme-Beaman A, Haile J, Jamieson A,
666 Meachen J, Lin AT, Schubert BW, Ameen C, Antipina EE, Bover P, Brace S, Carmagnini A,
667 Carøe C, Samaniego Castruita JA, Chatters JC, Dobney K, dos Reis M, Evin A, Gaubert P,
668 Gopalakrishnan S, Gower G, Heiniger H, Helgen KM, Kapp J, Kosintsev PA, Linderholm A,
669 Ozga AT, Presslee S, Salis AT, Saremi NF, Shew C, Skerry K, Taranenko DE, Thompson
670 M, Sablin MV, Kuzmin YV, Collins MJ, Sinding M-HS, Gilbert MTP, Stone AC, Shapiro B,
671 Van Valkenburgh B, Wayne RK, Larson G, Cooper A, Frantz LAF. 2021. Dire wolves were
672 the last of an ancient New World canid lineage. Nature 591(7848):87-91.
673 Rambaut A, Drummond AJ, Xie D, Baele G, Suchard MA. 2018. Posterior Summarization in
674 Bayesian Phylogenetics Using Tracer 1.7. Syst Biol 67(5):901-904.
675 Ramsden C, Melo FL, Figueiredo LM, Holmes EC, Zanotto PMA, the VC. 2008. High Rates of
676 Molecular Evolution in Hantaviruses. Mol Biol Evol 25(7):1488-1492.
677 Reimer PJ, Austin WEN, Bard E, Bayliss A, Blackwell PG, Bronk Ramsey C, Butzin M, Cheng H,
678 Edwards RL, Friedrich M, Grootes PM, Guilderson TP, Hajdas I, Heaton TJ, Hogg AG,
679 Hughen KA, Kromer B, Manning SW, Muscheler R, Palmer JG, Pearson C, van der Plicht

J, Reimer RW, Richards DA, Scott EM, Southon JR, Turney CSM, Wacker L, Adolphi F, Büntgen U, Capano M, Fahrni SM, Fogtmann-Schulz A, Friedrich R, Köhler P, Kudsk S, Miyake F, Olsen J, Reinig F, Sakamoto M, Sookdeo A, Talamo S. 2020. The IntCal20 Northern Hemisphere Radiocarbon Age Calibration Curve (0–55 cal kBP). Radiocarbon 62(4):725-757.

Rohland N, Harney E, Mallick S, Nordenfelt S, Reich D. 2015. Partial uracil-DNA-glycosylase treatment for screening of ancient DNA. Philos Trans R Soc Lond B Biol Sci 370(1660):20130624.

Rohland N, Reich D. 2012. Cost-effective, high-throughput DNA sequencing libraries for multiplexed target capture. Genome Res 22(5):939-946.

Salis AT, Bray SCE, Lee MSY, Heiniger H, Barnett R, Burns JA, Doronichev V, Fedje D, Golovanova L, Harington CR, Hockett B, Kosintsev P, Lai X, Mackie Q, Vasiliev S, Weinstock J, Yamaguchi N, Meachen J, Cooper A, Mitchell KJ. 2020. Lions and brown bears colonized North America in multiple synchronous waves of dispersal across the Bering Land Bridge. bioRxiv:2020.2009.2003.279117.

Salis AT, Gower G, Schubert BW, Soibelzon LH, Heiniger H, Prieto A, Prevosti FJ, Meachen J, Cooper A, Mitchell KJ. 2021. Ancient genomes reveal hybridisation between extinct short-faced bears and the extant spectacled bear (Tremarctos ornatus). bioRxiv:2021.2002.2005.429853.

Schubert M, Lindgreen S, Orlando L. 2016. AdapterRemoval v2: rapid adapter trimming, identification, and read merging. BMC Research Notes 9:88.

Seersholm FV, Werndly DJ, Grealy A, Johnson T, Keenan Early EM, Lundelius EL, Winsborough B, Farr GE, Toomey R, Hansen AJ, Shapiro B, Waters MR, McDonald G, Linderholm A, Stafford TW, Bunce M. 2020. Rapid range shifts and megafaunal extinctions associated with late Pleistocene climate change. Nature Communications 11(1):2770.

Stiller M, Molak M, Prost S, Rabeder G, Baryshnikov G, Rosendahl W, Münzel S, Bocherens H, Grandal-d'Anglade A, Hilpert B, Germonpré M, Stasyk O, Pinhasi R, Tintori A, Rohland N, Mohandesan E, Ho SYW, Hofreiter M, Knapp M. 2014. Mitochondrial DNA diversity and evolution of the Pleistocene cave bear complex. Quat Int 339-340:224-231.

Vershinina AO, Heintzman PD, Froese DG, Zazula G, Cassatt-Johnstone M, Dalén L, Der Sarkissian C, Dunn SG, Ermini L, Gamba C, Groves P, Kapp JD, Mann DH, Seguin-Orlando A, Southon J, Stiller M, Wooller MJ, Baryshnikov G, Gimranov D, Scott E, Hall E, Hewitson S, Kirillova I, Kosintsev P, Shidlovsky F, Tong H-W, Tiunov MP, Vartanyan S, Orlando L, Corbett-Detig R, MacPhee RD, Shapiro B. 2021. Ancient horse genomes reveal the timing and extent of dispersals across the Bering Land Bridge. Mol Ecol.

Waters MR, Stafford TW, Kooyman B, Hills LV. 2015. Late Pleistocene horse and camel hunting at the southern margin of the ice-free corridor: Reassessing the age of Wally's Beach, Canada. Proceedings of the National Academy of Sciences 112(14):4263.

718
719

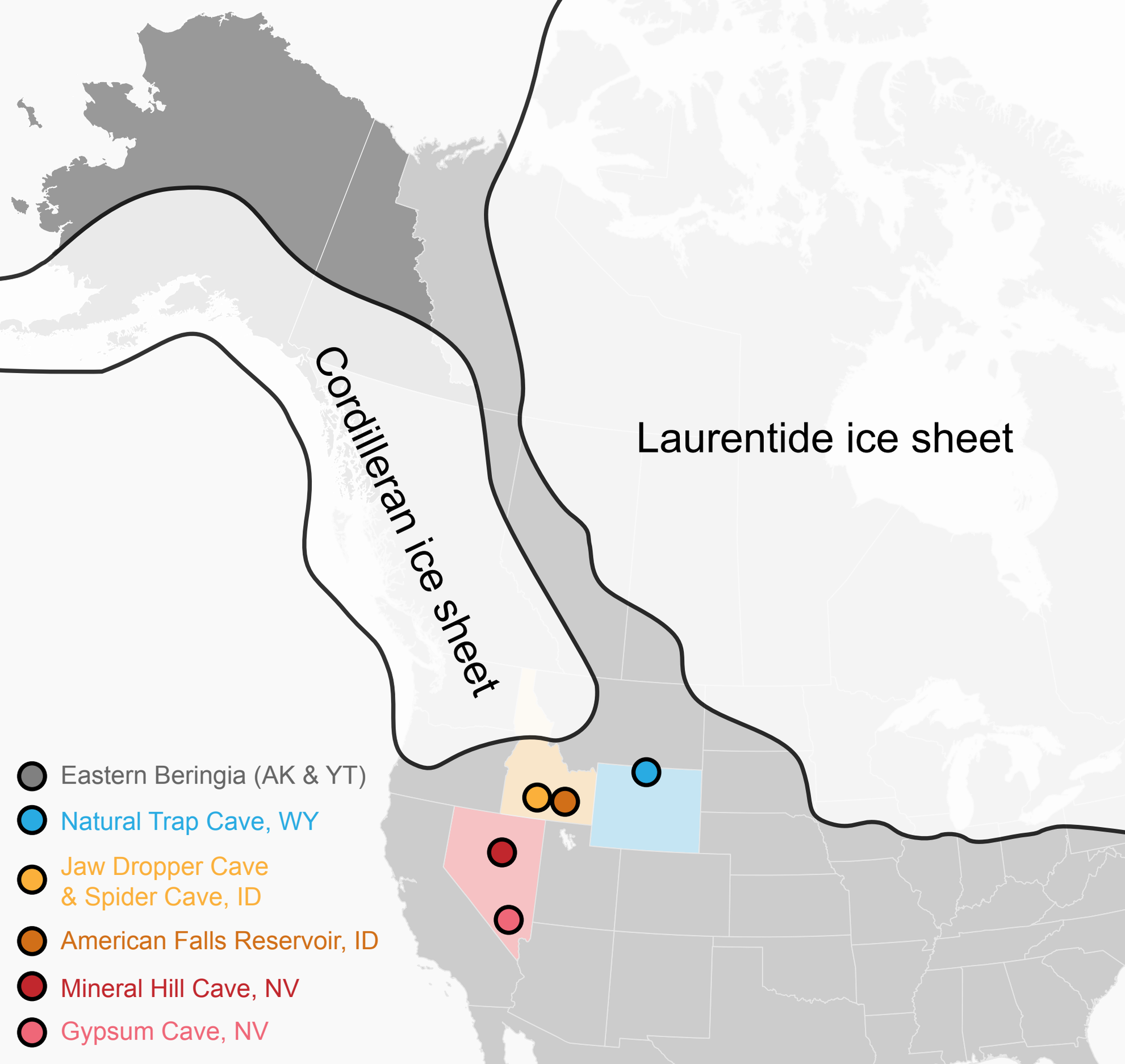
Cordilleran ice sheet
Laurentide ice sheet
Eastern Beringia (AK & YT)
Natural Trap Cave, WY
Jaw Dropper Cave
& Spider Cave, ID
American Falls Reservoir, ID
Mineral Hill Cave, NV
Gypsum Cave, NV

A

Minerall Hill Cave, NV
Gypsum Cave, NV
Natural Trap Cave, WY
Eastern Beringia

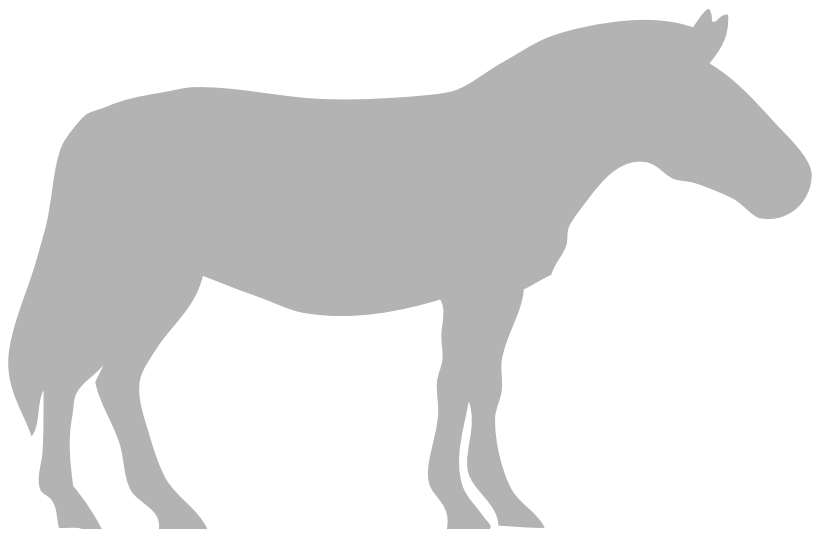

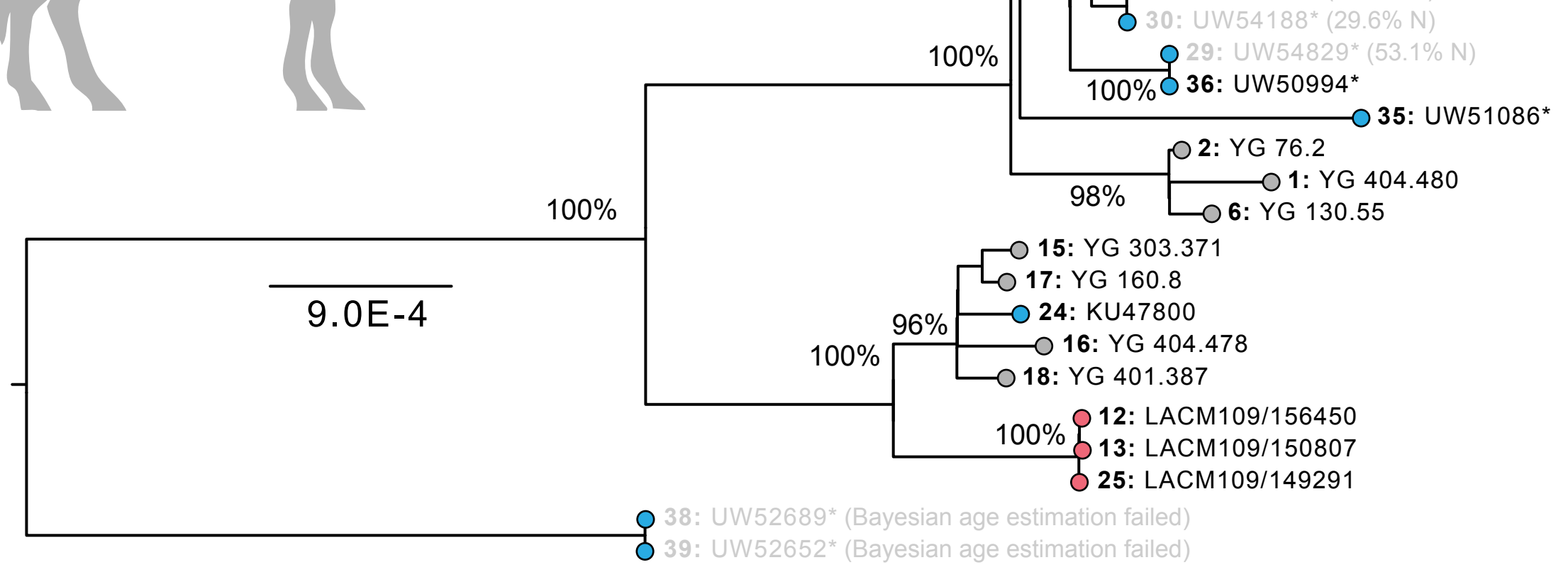

B

Gypsum Cave, NV
Natural Trap Cave, WY
Eastern Beringia

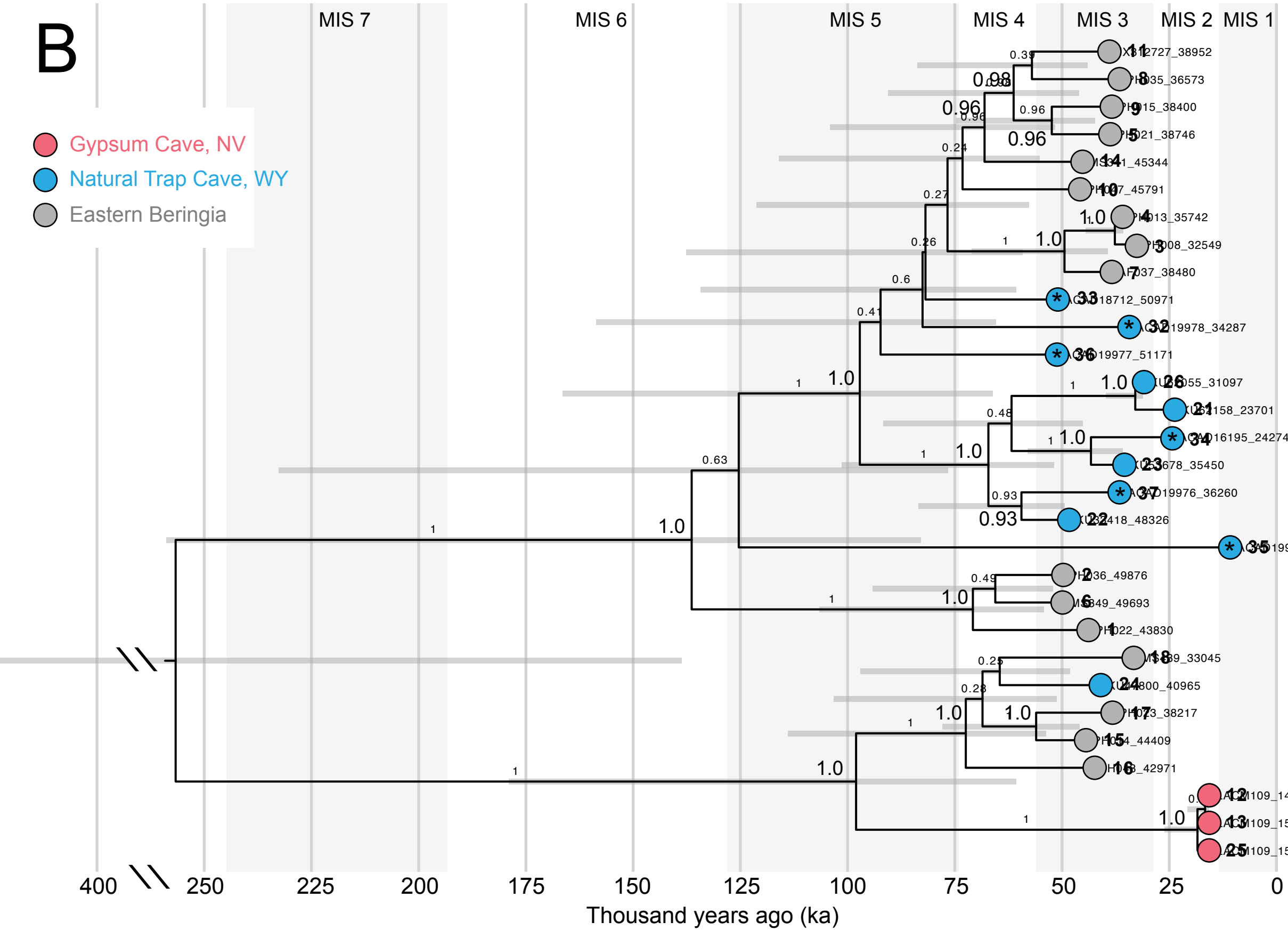

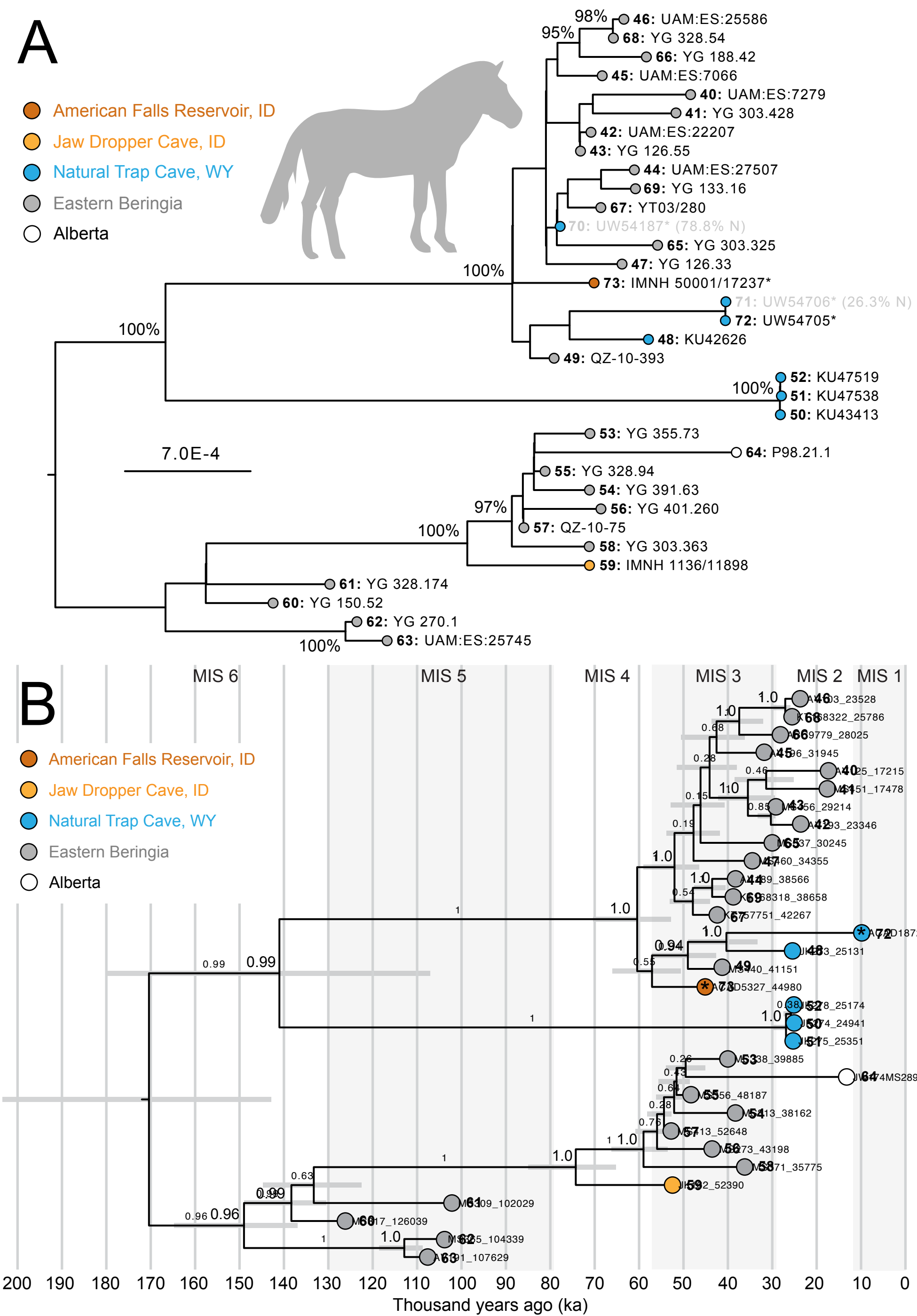
A
American Falls Reservoir, ID
Jaw Dropper Cave, ID
Natural Trap Cave, WY
Eastern Beringia
Alberta
98%
95%
46: UAM:ES:25586
68: YG 328.54
66: YG 188.42
45: UAM:ES:7066
40: UAM:ES:7279
41: YG 303.428
42: UAM:ES:22207
43: YG 126.55
44: UAM:ES:27507
69: YG 133.16
67: YT03/280
70: UW54187* (78.8% N)
65: YG 303.325
47: YG 126.33
100%
73: IMNH 50001/17237*
71: UW54706* (26.3% N)
72: UW54705*
48: KU42626
49: QZ-10-393
100%
100%
52: KU47519
51: KU47538
50: KU43413
7.0E-4
53: YG 355.73
64: P98.21.1
55: YG 328.94
54: YG 391.63
97%
56: YG 401.260
100%
57: QZ-10-75
58: YG 303.363
59: IMNH 1136/11898
61: YG 328.174
60: YG 150.52
62: YG 270.1
100%
63: UAM:ES:25745
B
MIS 6
MIS 5
MIS 4
MIS 3
MIS 2
MIS 1
American Falls Reservoir, ID
Jaw Dropper Cave, ID
Natural Trap Cave, WY
Eastern Beringia
Alberta
200 190 180 170 160 150 140 130 120 110 100 90 80 70 60 50 40 30 20 10 0
Thousand years ago (ka)

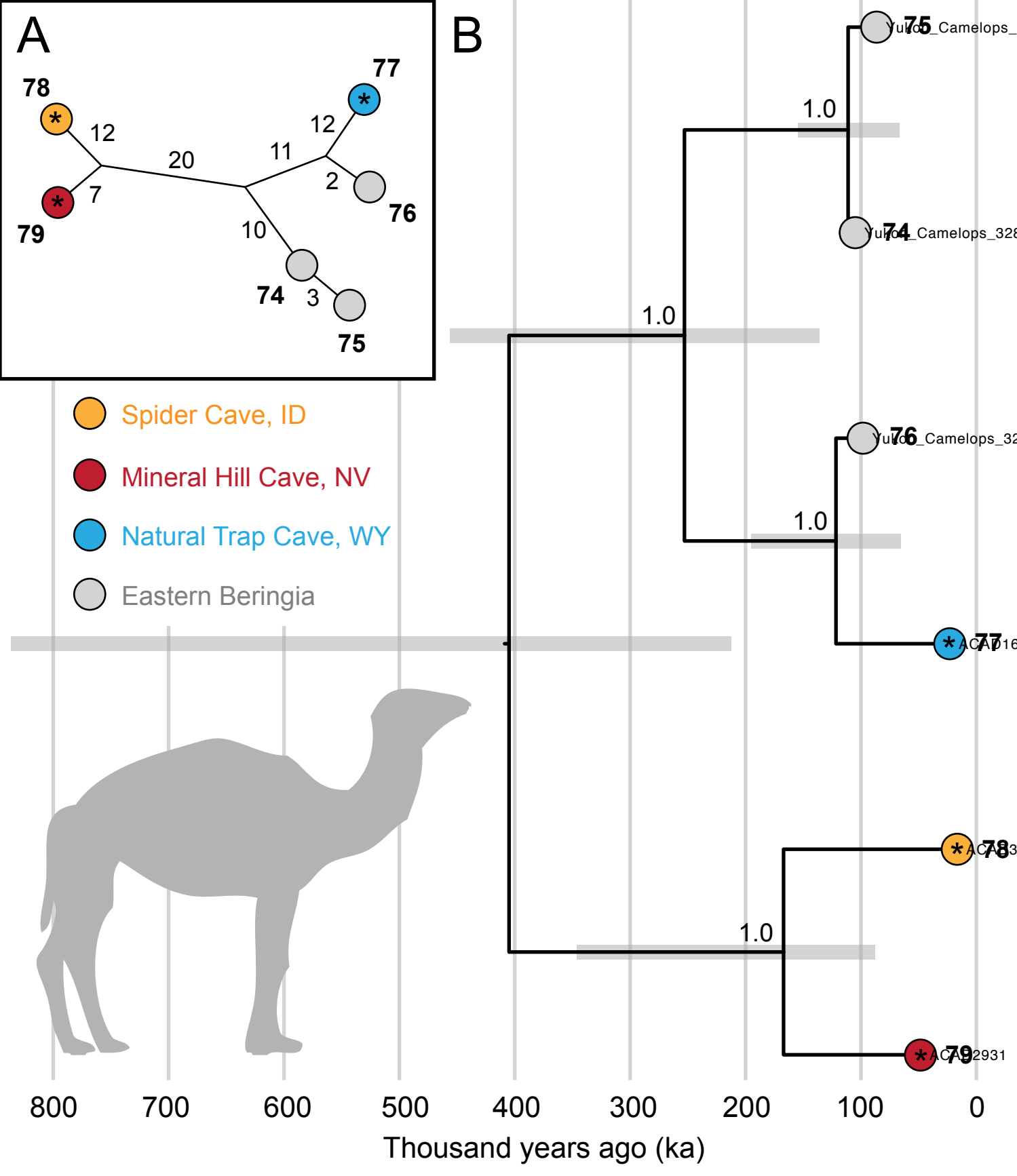
A
78
77
12
12
20
11
2
7
76
79
10
74
3
75
B
75
1.0
74
1.0
76
1.0
77
78
1.0
79
Spider Cave, ID
Mineral Hill Cave, NV
Natural Trap Cave, WY
Eastern Beringia
800
700
600
500
400
300
200
100
0
Thousand years ago (ka)

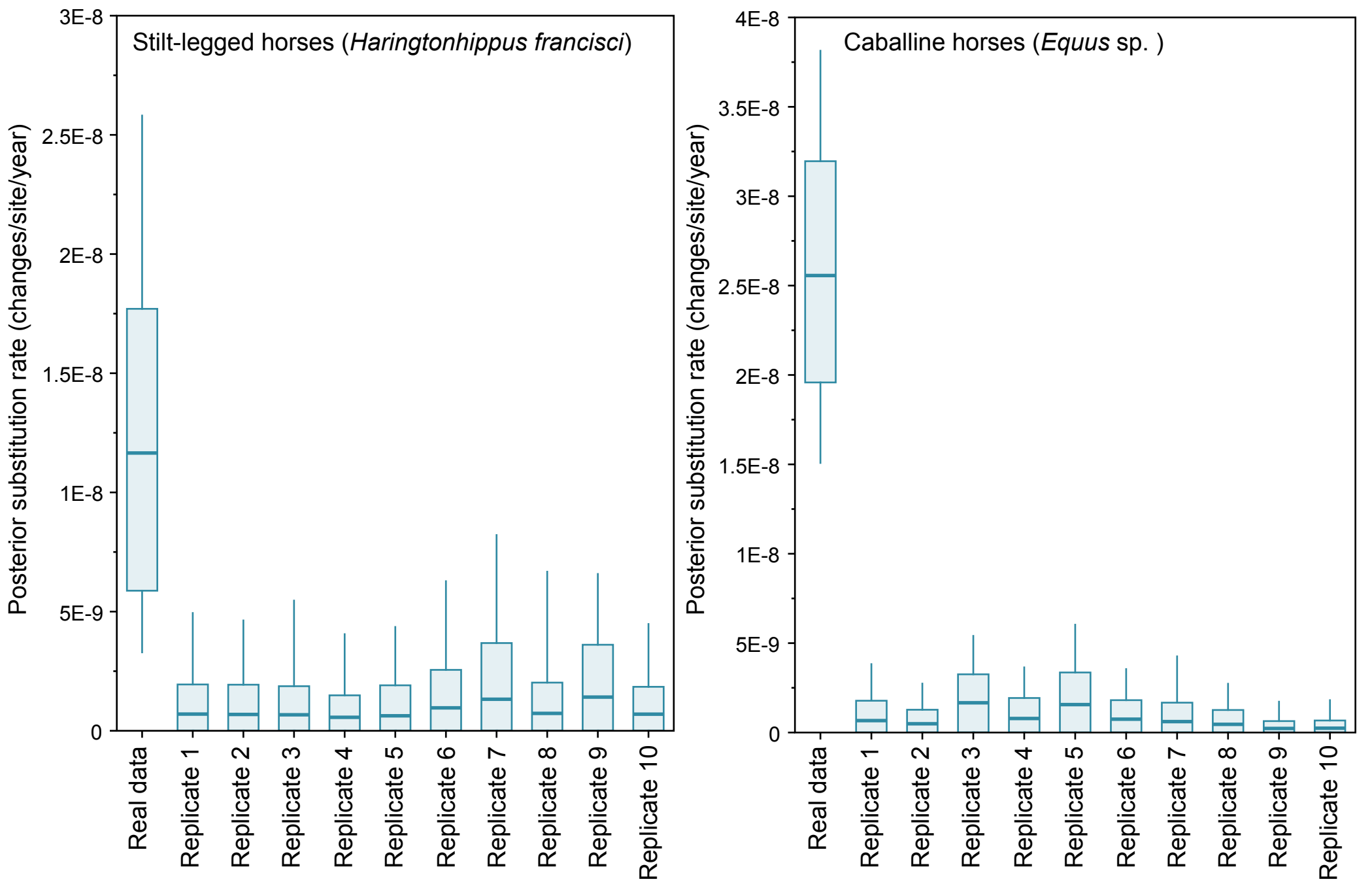
Stilt-legged horses (*Haringtonhippus francisci*)
Posterior substitution rate (changes/site/year)
3E-8
2.5E-8
2E-8
1.5E-8
1E-8
5E-9
0
Real data
Replicate 1
Replicate 2
Replicate 3
Replicate 4
Replicate 5
Replicate 6
Replicate 7
Replicate 8
Replicate 9
Replicate 10
Caballine horses (*Equus* sp.)
Posterior substitution rate (changes/site/year)
4E-8
3.5E-8
3E-8
2.5E-8
2E-8
1.5E-8
1E-8
5E-9
0
Real data
Replicate 1
Replicate 2
Replicate 3
Replicate 4
Replicate 5
Replicate 6
Replicate 7
Replicate 8
Replicate 9
Replicate 10

	Species	Provenance	DNA lab ID	Specimen ID	Collection data	GenBank accession	DNA data source	Library amplification PCR cycle number	Missing data (% N)	Depth of coverage, mean (x)	Depth of coverage, standard deviation (x)	Read length, mean (bp)	Read length, standard deviation (bp)
1	Haringtonhippus francisci	Hunker Creek, YT	PH022	YG 404.480		KT168334	Heintzman et al. 2017		0				
2	Haringtonhippus francisci	Hester Creek, YT	PH036	YG 76.2		KT168331	Heintzman et al. 2017		4,7				
3	Haringtonhippus francisci	Hunker Creek, YT	PH008	YG 404.205		KT168336	Heintzman et al. 2017		2,5				
4	Haringtonhippus francisci	Quartz Creek, YT	PH013	YG 130.6		KT168329	Heintzman et al. 2017		2,3				
5	Haringtonhippus francisci	Hunker Creek, YT	PH021	YG 29.169		KT168319	Heintzman et al. 2017		1,8				
6	Haringtonhippus francisci	Quartz Creek, YT	MS349	YG 130.55		KT168326	Heintzman et al. 2017		1,5				
7	Haringtonhippus francisci	Quartz Creek, YT	AF037	YG 402.235		KT168325	Heintzman et al. 2017		1,5				
8	Haringtonhippus francisci	Eureka Creek, YT	PH035	YG 417.13		KT168330	Heintzman et al. 2017		1,5				
9	Haringtonhippus francisci	Hunker Creek, YT	PH015	YG 404.662		KT168333	Heintzman et al. 2017		1,5				
10	Haringtonhippus francisci	Hunker Creek, YT	PH047	YG 404.663		KT168321	Heintzman et al. 2017		1,5				
11	Haringtonhippus francisci	Quartz Creek, YT	MS272	YG 401.268		JX312727	Vilstrup et al. 2013		1,5				
12	Haringtonhippus francisci	Gypsum Cave, NV	JK207	LACM109/156450		MF134657	Heintzman et al. 2017		1,7				
13	Haringtonhippus francisci	Gypsum Cave, NV	JW277; JK166	LACM109/150807		MF134655	Heintzman et al. 2017		1,6				
14	Haringtonhippus francisci	Eldorado Creek, YT	MS341	YG 303.1085		KT168328	Heintzman et al. 2017		1,5				
15	Haringtonhippus francisci	Eldorado Creek, YT	PH014	YG 303.371		KT168317	Heintzman et al. 2017		1,7				
16	Haringtonhippus francisci	Hunker Creek, YT	PH048	YG 404.478		KT168324	Heintzman et al. 2017		1,6				
17	Haringtonhippus francisci	Irish Gulch, YT	PH023	YG 160.8		KT168332	Heintzman et al. 2017		1,6				
18	Haringtonhippus francisci	Quartz Creek, YT	MS439	YG 401.387		KT168320	Heintzman et al. 2017		1,6				
19	Haringtonhippus francisci	Mineral Hill Cave, NV	JW328	NA		JX312726	Vilstrup et al. 2013		57				
20	Haringtonhippus francisci	Natural Trap Cave, WY	JK279	KU50817		MF134662	Heintzman et al. 2017		23,2				
21	Haringtonhippus francisci	Natural Trap Cave, WY	JW161; JK281	KU62158		MF134663	Heintzman et al. 2017		13,2				
22	Haringtonhippus francisci	Natural Trap Cave, WY	JK272	KU33418		MF134660	Heintzman et al. 2017		8,3				
23	Haringtonhippus francisci	Natural Trap Cave, WY	JK276	KU53678		MF134661	Heintzman et al. 2017		2,8				
24	Haringtonhippus francisci	Natural Trap Cave, WY	JK260	KU47800		MF134658	Heintzman et al. 2017		2,8				
25	Haringtonhippus francisci	Gypsum Cave, NV	JK167	LACM109/149291		MF134656	Heintzman et al. 2017		2,1				
26	Haringtonhippus francisci	Natural Trap Cave, WY	JW158; JK264	KU62055		MF134659	Heintzman et al. 2017		1,5				
27	Haringtonhippus francisci	Natural Trap Cave, WY	ACAD18710	UW54186	Excavated 2016; 490-495W/500-505N; 147	TBA	This study	13	85,7	1,1	1,3	76,6	23
28	Haringtonhippus francisci	Natural Trap Cave, WY	ACAD18713	UW54828	Excavated 2016; >520W/480-485N; 1478.3	TBA	This study	12	83,7	1,2	1,4	75,3	23,3
29	Haringtonhippus francisci	Natural Trap Cave, WY	ACAD18711	UW54829	Excavated 2016; >520W/485-490N; 1479.2	TBA	This study	14	53,1	2,7	2,2	77,4	24,1
30	Haringtonhippus francisci	Natural Trap Cave, WY	ACAD18727	UW54188	Excavated 2016	TBA	This study	13	29,6	6	5	68,5	21,8
31	Haringtonhippus francisci	Natural Trap Cave, WY	ACAD18155	UW52685	Excavated 2015	TBA	This study	11	22,5	6,6	4,9	85,8	30,7
32	Haringtonhippus francisci	Natural Trap Cave, WY	ACAD19978	UW50918	Excavated 2014; 500-505W/495-500N; 140	TBA	This study	12	14,9	16,4	13,2	77,7	22,6
33	Haringtonhippus francisci	Natural Trap Cave, WY	ACAD18712	UW54704	Excavated 2016; 495-500W/500-505N; 147	TBA	This study	12	13,3	14,4	11,7	69,4	20,8
34	Haringtonhippus francisci	Natural Trap Cave, WY	ACAD16195	UW51530	Excavated 2014; 500-505W/495-500N	TBA	This study	15	5,8	103,8	63,5	80,2	28,3
35	Haringtonhippus francisci	Natural Trap Cave, WY	ACAD19979	UW51086	Excavated 2014; 525-530W/480-485N; appr	TBA	This study	12	2,1	95,9	59,2	77,3	23
36	Haringtonhippus francisci	Natural Trap Cave, WY	ACAD19977	UW50994	Excavated 2014; 525-530W/480-485N; appr	TBA	This study	15	2	120,3	60,6	77,2	23
37	Haringtonhippus francisci	Natural Trap Cave, WY	ACAD19976	UW51648	Excavated 2015; 515-520W/475-480N; 147	TBA	This study	11	1,9	277,8	167,7	82,5	22,5
38	Haringtonhippus francisci	Natural Trap Cave, WY	ACAD18156	UW52689	Excavated 2015; test pit 1; 77 cm below sur	TBA	This study	14	2,5	103,8	63,5	80,2	28,3
39	Haringtonhippus francisci	Natural Trap Cave, WY	ACAD17385	UW52652	Excavated 2015; test pit 1; 69 cm below sur	TBA	This study	12	2,8	131,1	85,4	76	23,6
40	Equus sp.	Lost Chicken Creek, AK	AV125	UAM:ES:7279		MW846121	Vershinina et al. 2021		0				
41	Equus sp.	Eldorado Creek, YT	MS451	YG 303.428		MW846165	Vershinina et al. 2021		2,3				
42	Equus sp.	Fairbanks, AK	AV193	UAM:ES:22207		MW846133	Vershinina et al. 2021		0,2				
43	Equus sp.	Irish Gulch, YT	MS456	YG 126.55		MW846166	Vershinina et al. 2021		1,5				
44	Equus sp.	Fairbanks, AK	AV189	UAM:ES:27507		MW846130	Vershinina et al. 2021		0,1				
45	Equus sp.	Lost Chicken Creek, AK	AV196	UAM:ES:7066		MW846134	Vershinina et al. 2021		0,9				
46	Equus sp.	Fairbanks, AK	AV103	UAM:ES:25586		MW846110	Vershinina et al. 2021		0,1				
47	Equus sp.	Irish Gulch, YT	MS460	YG 126.33		MW846167	Vershinina et al. 2021		7,4				
48	Equus sp.	Natural Trap Cave, WY	JK273	KU42626		MW846143	Vershinina et al. 2021		0,9				
49	Equus sp.	Quartz Creek, YT	MS440	QZ-10-393		MW846164	Vershinina et al. 2021		4,1				
50	Equus sp.	Natural Trap Cave, WY	JK274	KU43413		MW846144	Vershinina et al. 2021		7,1				
51	Equus sp.	Natural Trap Cave, WY	JK275	KU47538		MW846145	Vershinina et al. 2021		0,5				
52	Equus sp.	Natural Trap Cave, WY	JK278	KU47519		MW846146	Vershinina et al. 2021		2				
53	Equus sp.	Green Gulch, YT	MS338	YG 355.73		MW846159	Vershinina et al. 2021		0,1				
54	Equus sp.	Quartz Creek, YT	MS313	YG 391.63		MW846154	Vershinina et al. 2021		0,1				
55	Equus sp.	Hunker Creek, YT	MS356	YG 328.94		MW846160	Vershinina et al. 2021		0,1				
56	Equus sp.	Quartz Creek, YT	MS273	YG 401.260		MW846152	Vershinina et al. 2021		0,1				
57	Equus sp.	Quartz Creek, YT	MS413	QZ-10-75		MW846163	Vershinina et al. 2021		0,6				
58	Equus sp.	Eldorado Creek, YT	MS371	YG 303.363		MW846162	Vershinina et al. 2021		0,1				
59	Equus sp.	Jaw Dropper Cave, ID	JK162	IMNH 1136/11898		MW846142	Vershinina et al. 2021		0,1				
60	Equus sp.	Thistle Creek, YT	MS317	YG 150.52		MW846155	Vershinina et al. 2021		0,2				
61	Equus sp.	Hunker Creek, YT	MS309	YG 328.174		MW846153	Vershinina et al. 2021		0				
62	Equus sp.	Lucky Lady, YT	MS365	YG 270.1		MW846161	Vershinina et al. 2021		0,1				
63	Equus sp.	Engineer Creek, YT	AV191	UAM:ES:25745		MW846132	Vershinina et al. 2021		14,2				
64	Equus sp.	Grand Prairie, AB	JW174; MS289	P98.21.1		MW846147	Vershinina et al. 2021		0,6				
65	Equus sp.	Eldorado Creek, YT	MS337; JK141	YG 303.325		MW846158	Vershinina et al. 2021		0,7				
66	Equus sp.	Irish Gulch, YT	ABC9779	YG 188.42; YT03-40		MW846090	Vershinina et al. 2021		0,1				
67	Equus sp.	Thistle Creek, YT	JW119; MS292	YT03/280		KT757751	Orlando et al. 2013		1,5				
68	Equus sp.	Hunker Creek, YT	MS316	YG 328.54		KT168322	Heintzman et al. 2017		1,5				
69	Equus sp.	Whitman Gulch, YT	MS352	YG 133.16		KT168318	Heintzman et al. 2017		1,5				
70	Equus sp.	Natural Trap Cave, WY	ACAD18715	UW54187	Excavated 2016; 490-495W/500-505N; 147	TBA	This study	12	78,8	0,8	1,1	78	22,5
71	Equus sp.	Natural Trap Cave, WY	ACAD18716	UW54706	Excavated 2016; 495-500W/495-500N; 147	TBA	This study	13	26,3	3,7	3	76,9	23,6
72	Equus sp.	Natural Trap Cave, WY	ACAD18728	UW54705	Excavated 2016; 495-500W/495-500N; 147	TBA	This study	15	2,7	45	23,2	76,6	23,2
73	Equus sp.	American Falls Reservoir, ID	ACAD5327	IMNH 50001/17237	N/A	TBA	This study	17	5,4	16,3	9	73	22
74	Camelops cf. hesternus	Hunker Creek, YT	NA	YG 328.21		KR822421	Heintzman et al. 2015		1,9				
75	Camelops cf. hesternus	Hunker Creek, YT	NA	YG 29.199		KR822422	Heintzman et al. 2015		1,9				
76	Camelops cf. hesternus	Hunker Creek, YT	NA	YG 328.23		KR822420	Heintzman et al. 2015		1,9				
77	Camelops cf. hesternus	Natural Trap Cave, WY	ACAD16197	UW51516	Excavated 2014; 520W SW corner/485N SW	TBA	This study	RPA; 40 min	52,6	2	2,1	75,7	29,2
78	Camelops cf. hesternus	Spider Cave, ID	ACAD342	IMNH 2027/14846; IMNH 2027/1846	N/A	TBA	This study	12	3,6	44,6	30,3	83,9	30,3
79	Camelops cf. hesternus	Mineral Hill Cave, NV	ACAD2931	TP2-SL-1	N/A	TBA	This study	12	53,5	1,9	2,2	76,7	24

Reference sequence	14C lab code	14C lab number	14C age	±	Median (yrs calBP; IntCal 20)	Mean (yrs calBP; IntCal 20)	Sigma; IntCal 20	δ13C	Dated material	Pretreatment	14C data source	Median	Mean	95% HPD L	95% HPD U	Notes
	UCIAMS	114018	40600	1100	43830	43921	842				Heintzman et al. 2017	25031	25187	25	47158	Passed 14C cross-validation
	UCIAMS	114013	46600	2200	49876	50083	2415				Heintzman et al. 2017	62023	66826	42598	109370	Passed 14C cross-validation
	UCIAMS	114020	28390	240	32549	32560	404				Heintzman et al. 2017	32015	30596	14899	41273	Passed 14C cross-validation
	UCIAMS	114015	31360	340	35742	35737	340				Heintzman et al. 2017	33440	33433	19244	43975	Passed 14C cross-validation
	UCIAMS	114014	33840	460	38746	38697	674				Heintzman et al. 2017	33155	31628	6849	47798	Passed 14C cross-validation
	UCIAMS	125771	46500	1900	49693	49953	2303				Heintzman et al. 2017	48578	48938	14352	72120	Passed 14C cross-validation
	UCIAMS	114037	33630	450	38480	38452	654				Heintzman et al. 2017	41369	43022	15700	73443	Passed 14C cross-validation
	UCIAMS	114021	32190	370	36573	36607	428				Heintzman et al. 2017	39943	39296	14993	59520	Passed 14C cross-validation
	UCIAMS	114019	33560	440	38400	38379	645				Heintzman et al. 2017	33931	32593	6497	50040	Passed 14C cross-validation
	UCIAMS	114024	42900	1400	45791	46056	1554				Heintzman et al. 2017	57496	61600	27668	11160	Passed 14C cross-validation
	CAMS	157469	33930	350	38952	38861	557				Heintzman et al. 2017	33932	32865	7306	51171	Passed 14C cross-validation
	UCIAMS	163269	13065	35	15662	15660	70				Heintzman et al. 2017	15833	16135	3118	26573	Passed 14C cross-validation
	OxA	13838	13070	55	15667	15664	95				Heintzman et al. 2017	15727	16017	3837	26484	Passed 14C cross-validation
	UCIAMS	125770	42500	1200	45344	45504	1199				Heintzman et al. 2017	44437	45588	10064	75427	Passed 14C cross-validation
	UCIAMS	114016	41400	1200	44409	44530	1082				Heintzman et al. 2017	34584	33557	15125	47595	Passed 14C cross-validation
	UCIAMS	114022	39260	900	42971	43107	613				Heintzman et al. 2017	27965	27883	463	4760	Passed 14C cross-validation
	UCIAMS	114017	33400	430	38217	38213	646				Heintzman et al. 2017	45138	45980	21486	64742	Passed 14C cross-validation
	CAMS	161727	28740	570	33045	33028	721				Heintzman et al. 2017	48541	51079	21249	83225	Passed 14C cross-validation
												35577	36340	161	66543	Excluded from final BEAST
												55724	59735	34735	96277	Excluded from final BEAST
												23772	24860	21	50429	
												48397	46945	32	80373	
												35521	36129	27	66430	
												41036	41556	3038	71429	
												15745	16176	3422	25823	
												31168	32624	91	61521	
KT168321												26846	36238	4	108000	Excluded from final BEAST
KT168321												57211	61226	4606	120750	Excluded from final BEAST
KT168321												62102	63396	9666	108500	Excluded from final BEAST
KT168321												54568	56870	19067	98496	Excluded from final BEAST
KT168321												26016	28415	5	59522	Excluded from final BEAST
KT168321												34358	35088	2	62674	
KT168321												51042	52154	12387	86248	
KT168321												24345	25275	40	50536	
KT168321												10858	13149	3	32793	
KT168321												51242	51330	7251	84445	
KT168321												36331	35978	266	64507	
KT168321																BEAST age estimation faile
KT168321																BEAST age estimation faile
	UCIAMS	196058	14165	50	17215	17217	84				Vershinina et al. 2021	9495	10313	0,1	22582	Passed 14C cross-validation
	CAMS_LLNL	161729	14340	90	17478	17499	176				Vershinina et al. 2021	13976	14441	10,8	28639	Passed 14C cross-validation
	UCIAMS	208133	19390	60	23346	23404	191				Vershinina et al. 2021	27615	27203	17117	37129	Passed 14C cross-validation
	CAMS_LLNL	161730	24930	350	29214	29240	398				Vershinina et al. 2021	27254	27533	18136	38226	Passed 14C cross-validation
	UCIAMS	208139	33650	290	38566	38518	506				Vershinina et al. 2021	35487	34687	20554	46520	Passed 14C cross-validation
	UCIAMS	208141	28020	150	31945	32022	302				Vershinina et al. 2021	36458	36537	19460	54721	Passed 14C cross-validation
	UCIAMS	184441	19610	70	23528	23567	138				Vershinina et al. 2021	23639	22940	11868	32020	Passed 14C cross-validation
	CAMS_LLNL	166299	29860	620	34355	24339	687				Vershinina et al. 2021	30276	29850	5208	51647	Passed 14C cross-validation
	CAMS_LLNL	173976	20840	90	25131	25129	124				Vershinina et al. 2021	29464	28715	1335	48558	Passed 14C cross-validation
	CAMS_LLNL	161546	36290	1460	41151	41113	1224				Vershinina et al. 2021	57865	60495	32055	92775	Passed 14C cross-validation
	CAMS_LLNL	174029	20690	110	24941	24923	168				Vershinina et al. 2021	25205	24998	15690	34637	Passed 14C cross-validation
	CAMS_LLNL	174093	21000	110	25351	25363	157				Vershinina et al. 2021	24952	24736	16282	33421	Passed 14C cross-validation
	OxA	14910	20880	90	25174	25184	132				Vershinina et al. 2021	25170	25007	16801	33848	Passed 14C cross-validation
	CAMS_LLNL (Collagen UAF)	157455	34690	390	39885	39908	409				Vershinina et al. 2021	40318	39917	20436	57319	Passed 14C cross-validation
	CAMS_LLNL (Collagen UAF)	157443	33350	340	38162	38169	574				Vershinina et al. 2021	43828	43845	24757	62571	Passed 14C cross-validation
												48258	49890	36742	67935	
	CAMS_LLNL (Collagen UAF)	157470	39740	720	43198	43292	529				Vershinina et al. 2021	34902	34312	14342	51474	Passed 14C cross-validation
	CAMS_LLNL	161722	>44400	inf	NA	NA	NA				Vershinina et al. 2021	52719	53555	42420	65393	
	CAMS_LLNL (Collagen UAF)	157475	31400	260	35775	35772	263				Vershinina et al. 2021	45627	45616	22636	66496	Passed 14C cross-validation
	CAMS_LLNL	175552	14225	40	17275	17264	89				Vershinina et al. 2021	52461	53137	33291	74672	Failed age cross-validation
	CAMS_LLNL (Collagen UAF)	157446	>53700	inf	NA	NA	NA				Vershinina et al. 2021	126110	130730	77367	190580	
	CAMS_LLNL (Collagen UAF)	157440	>53700	inf	NA	NA	NA				Vershinina et al. 2021	102100	105320	63424	153610	
	CAMS_LLNL (Collagen UAF)	157497	>52400	inf	NA	NA	NA				Vershinina et al. 2021	104410	113180	59672	190680	
	UCIAMS	208138	>52200	inf	NA	NA	NA				Vershinina et al. 2021	107700	119740	48410	215500	
	OxA	14270	11200	90	13115	13105	96				Lorenzen et al. 2011	7311	8709	3,2	21436	Passed 14C cross-validation
	CAMS_LLNL	157454	26020	140	30245	30285	183				Vershinina et al. 2021	27255	26385	2255	45820	Passed 14C cross-validation
	OxA	17686	23920	100	28025	28051	165				Lorenzen et al. 2011	17140	16887	524	29966	Passed 14C cross-validation
												42338	42473	32780	52353	
	CAMS	157445	21420	80	25786	25784	73				Heintzman et al. 2017	26081	26052	17136	35632	Passed 14C cross-validation
	CAMS	157487	33760	400	38658	38609	608				Heintzman et al. 2017	35361	34608	19993	46338	Passed 14C cross-validation
KT168318												35245	36354	7044	69186	Excluded from final BEAST
KT168318												9895	10901	7	24450	Excluded from final BEAST
KT168318												9780	10585	1	22986	
KT168318	OxA	37893	>49000	inf	NA	NA	NA	-17,52	Bone	Collagen ultrafiltration	This study	45051	45210	26282	64909	Registered taxonomic ID in
	UCIAMS	117244	>51,700	inf	NA	NA	NA				Heintzman et al. 2015	98214	99689	58983	147500	
	UCIAMS	72416	>49,900	inf	NA	NA	NA				Heintzman et al. 2015	86417	87987	50068	127010	
	UCIAMS	117246	>51,700	inf	NA	NA	NA				Heintzman et al. 2015	105030	105240	67107	149520	
KR822421	OxA	37991	20730	120	23042	23022	177	-18,18	Bone	Collagen ultrafiltration	This study					
KR822421	OxA	37878	15130	70	16516	16516	119	-18,79	Bone	Collagen ultrafiltration	This study					DNA analysed from a phala
KR822421	NA	NA	44600	3000	48399	48764	2977				Hockett & Dillingham, 2004					

n
n
n
n
n
n
n
n
n
n
n
n
n
n
n
n
n
n
analysis due to data missingness
analysis due to data missingness

analysis due to data missingness
analysis due to data missingness
analysis due to data missingness
analysis due to data missingness
analysis due to data missingness

d. Sample excluded from final BEAST analysis.
d. Sample excluded from final BEAST analysis.
n
n
n
n
n
n
n
n
n
n
n
n
n
n
n
n
n

n
: 14C falls outside HPD. Possibly contaminated with younger C. Estimated median value used in final BEAST analyses.

n
n
n

n
n
analysis due to data missingness
analysis due to data missingness

correct. Originally identified as *Panthera atrox*, but revised to *Equus* following genetic analysis by Salis et al. 2020.

ınx (IMNH 2027/14846). Radiocarbon date obtained from a left tibia (IMNH 2027/1846) presumed to come from the same individual.